NANO LETTERS

2007
Vol. 7, No. 8
2422−2427

Size and Surface Effects on the MRI Relaxivity of Manganese Ferrite Nanoparticle Contrast Agents

Ulrich I. Tromsdorf,[†,#] Nadja C. Bigall,[†,#] Michael G. Kaul,[‡] Oliver T. Bruns,[§] Marija S. Nikolic,[†] Birgit Mollwitz,[§] Ralph A. Sperling,[||] Rudolph Reimer,[⊥] Heinz Hohenberg,[⊥] Wolfgang J. Parak,[||] Stephan Förster,[†] Ulrike Beisiegel,[§] Gerhard Adam,[‡] and Horst Weller*[,†]

Institute of Physical Chemistry, University of Hamburg, Grindelallee 117, 20146 Hamburg, Germany, Department of Diagnostic and Interventional Radiology, University Medical Center Hamburg-Eppendorf, Martinistrasse 52, 20246 Hamburg, Germany, Department of Biochemistry and Molecular Biology II: Molecular Cell Biology, University Medical Center Hamburg-Eppendorf, Martinistrasse 52, 20246 Hamburg, Germany, Ludwig-Maximilians-University, Center of NanoScience, Amalienstrasse 54, 80799 Munich, Germany, and Department of Electron Microscopy and Micro Technology, Heinrich-Pette Institute, Martinistrasse 52, 20251 Hamburg, Germany

Received May 11, 2007; Revised Manuscript Received July 2, 2007

ABSTRACT

Superparamagnetic $MnFe_2O_4$ nanocrystals of different sizes were synthesized in high-boiling ether solvent and transferred into water using three different approaches. First, we applied a ligand exchange in order to form a water soluble polymer shell. Second, the particles were embedded into an amphiphilic polymer shell. Third, the nanoparticles were embedded into large micelles formed by lipids. Although all approaches lead to effective negative contrast enhancement, we observed significant differences concerning the magnitude of this effect. The transverse relaxivity, in particular r_2*, is greatly higher for the micellar system compared to the polymer-coated particles using same-sized nanoparticles. We also observed an increase in transverse relaxivities with increasing particle size for the polymer-coated nanocrystals. The results are qualitatively compared with theoretical models describing the dependence of relaxivity on the size of magnetic spheres.

Magnetic nanoparticles became more and more important for applications in biotechnology and biomedicine[1] as well as technical ones like magnetic data storage[2] over the past few years. Examples are magnetothermal therapy[3,4] or in vivo imaging.[5−7] Here we present the synthesis and potential use of superparamagnetic manganese ferrite nanocrystals ($MnFe_2O_4$) as contrast agents in magnetic resonance imaging (MRI).[8] Whereas enormous progress has been achieved in the technological development of MRI, including sophisticated pulse sequences for image generation, the development of chemical contrast agents still has a great potential for improvement. In particular, T_2 contrast agents under clinical use consist of very polydisperse and aggregated iron oxide nanoparticles. Recent investigations impressively show that the contrast enhancement of nanoparticles is strongly determined by their size, surface properties, and the degree of aggregation.[9−11] The aim of this work is to clearly distinguish between these effects by using monodisperse samples of 3−18 nm $MnFe_2O_4$ particles and to subject these samples to various methods of surface functionalization and compartmentalization in lipid micelles. We will also distinguish between the impact of these effects in the various pulse sequence modes for the detection of both the transverse relaxation (T_2 process) and the effective transverse relaxation (T_2* process).

The MRI signal that is detected after the excitation of magnetic moments by a radio frequency (rf) pulse is determined by the examined object and the imaging sequence. The imaging sequence is weighting the impact of the net magnetization of hydrogen atoms and the relaxation mechanisms. The first mechanism describes the relaxation

* Corresponding author. E-mail: weller@chemie.uni-hamburg.de.
[†] Institute of Physical Chemistry, University of Hamburg.
[‡] Department of Diagnostic and Interventional Radiology, University Medical Center Hamburg-Eppendorf.
[§] Department of Biochemistry and Molecular Biology II: Molecular Cell Biology, University Medical Center Hamburg-Eppendorf.
[||] Ludwig-Maximilians-University, Center of NanoScience.
[⊥] Department of Electron Microscopy and Micro Technology, Heinrich-Pette Institute.
[#] These authors contributed equally to this work.

10.1021/nl071099b CCC: $37.00
Published on Web 07/20/2007

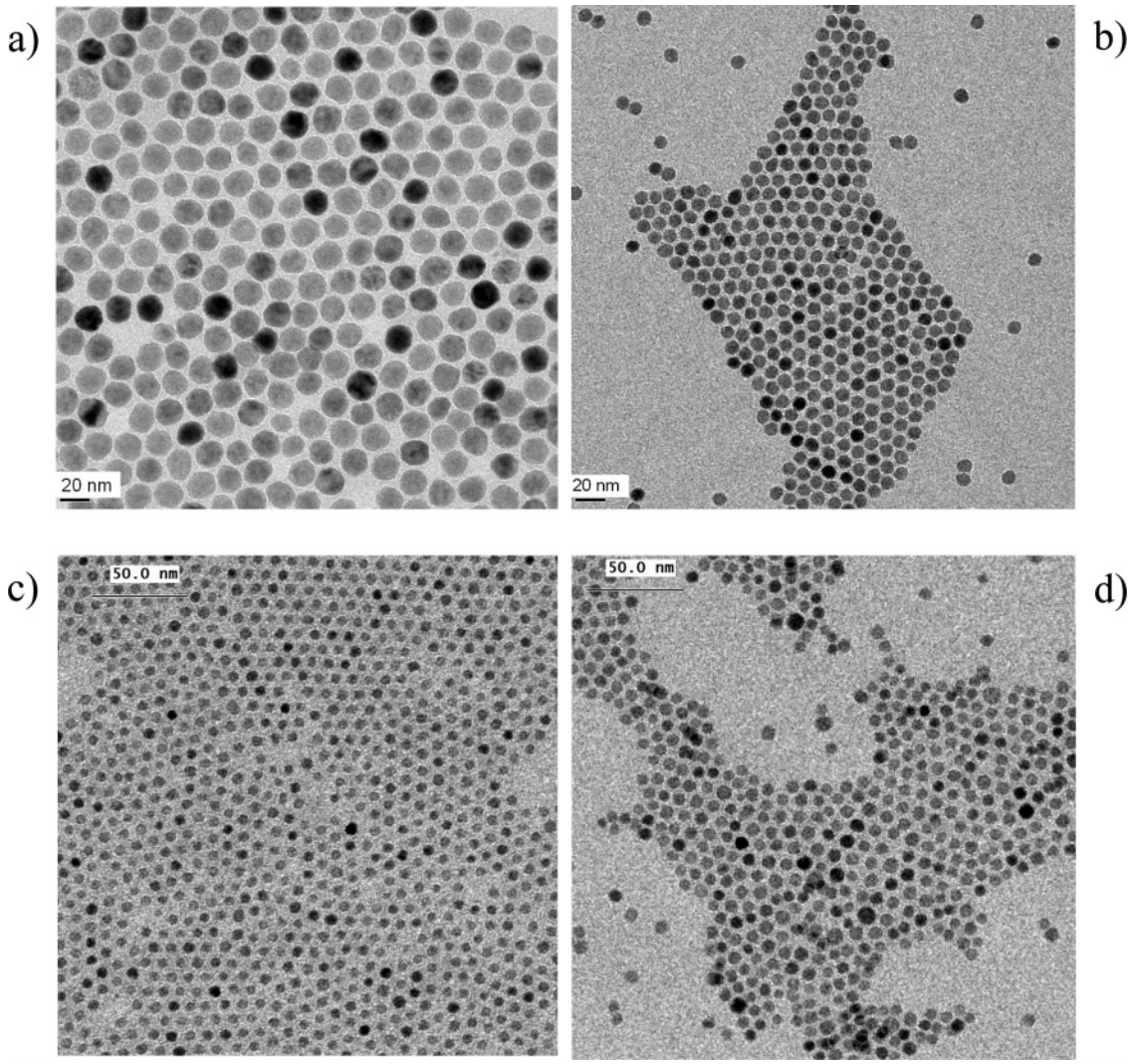

Figure 1. TEM image of 18 nm (a) and 9 nm (b) monodisperse samples (less than 10% standard deviation) of $MnFe_2O_4$ nanocrystals as well as fractions of 6 nm (c) and 7.5 nm (d) manganese-doped iron oxide nanoparticles (standard deviation about 10%).

to the equilibrium occupancy of α and β spins and is referred to as longitudinal or spin−lattice relaxation. This process is characterized by the time constant T_1. The second mechanism characterizes the dephasing of coherent spins that are generated during the rf pulse and is referred to as transverse or spin−spin relaxation with the time constant T_2. Furthermore, the effective transverse relaxation time T_2* describes the relaxation increase due to additional inhomogeneities in the magnetic field. These inhomogeneities can be caused by the nonperfect homogeneous magnetic field itself or by susceptibility effects implied by tissue interfaces with different magnetization or by para- and ferromagnetic materials. Therefore, T_2* can be significantly smaller than T_2. Whereas the T_1 relaxation leads to an increase in signal intensity and thus causing positive contrast, the T_2 and T_2* processes result in signal loss and negative contrast with conventional imaging techniques. Because superparamagnetic nanoparticles greatly shorten T_2 and T_2* due to their large magnetic moment they commonly act as negative contrast agents. This effect is quantified in the concentration-independent transverse relaxivities r_2 and r_2*, that is, the ability of the contrast agent to shorten T_2 and T_2*, respectively, per millimolar concentration of paramagnetic ions. $MnFe_2O_4$ nanoparticles have recently been demonstrated to act as powerful negative contrast agents[11] and were even stronger then magnetite.

To synthesize the nanoparticles, we used the high-temperature organometallic synthesis reported by Kang et al., which yields highly crystalline and monodisperse nanocrystals with no tendency to agglomerate.[12a] This method is based on thermal decomposition of $Fe(CO)_5$ and $Mn_2(CO)_{10}$, resulting in the formation of FeMn alloy nanoparticles followed by oxidation with trimethylamine-*N*-oxide. The synthesis yielded nearly monodisperse nanoparticles (less than 10% standard deviation), which were characterized by transmission electron microscopy (TEM) (Figure 1) and X-ray diffraction (XRD) (Supporting Information Figure S1). EDX measurements indicated that the ratio of iron and manganese was almost 2:1. By varying the ratio of initial precursor to oleic acid, particles between 3 and 18 nm could be synthesized. Moreover, we used a hot injection method based on a modification of ref 12b. The high-temperature reaction of iron(III)acetylacetonate and manganese(II)acetylacetonate with 1,2-hexadecanediol in the presence of oleic acid and oleyl amine yielded polydisperse samples that could

Scheme 1. Schematic Illustration of the Phase Transfer Approaches: Ligand Exchange of Oleic Acid against Water Soluble Polymer (above), Coating of Individual Nanoparticles with Amphiphilic Polymer and Embedding into Lipid Micelles (below)

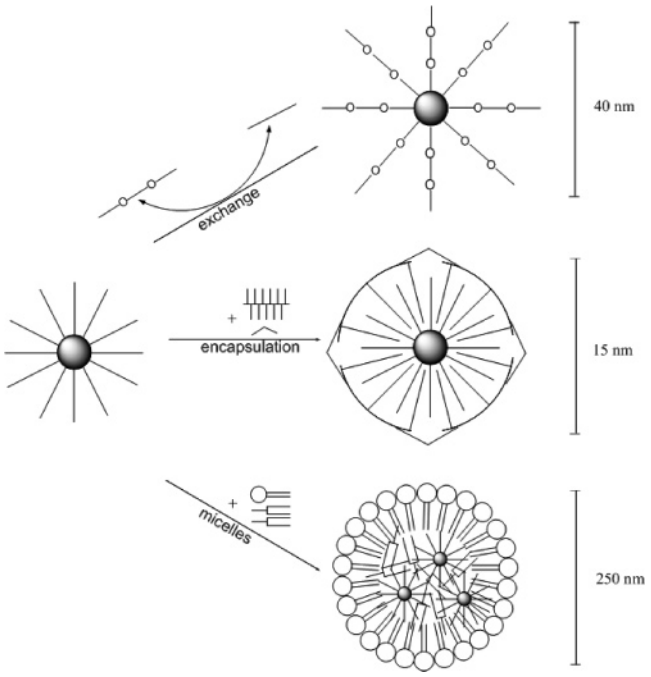

be easily separated into size fractions of 4.5, 6, and 7.5 nm (standard deviation approximately 10%), respectively (Figure 1). Moreover, the ratio of manganese to iron decreased from 0.32 for the 4.5 nm particles to 0.12 for 7.5 nm particles.

Because of the synthesis conditions, the particles are hydrophobic and thus not soluble in aqueous media. To transfer the nanoparticles into water, we used different approaches. In the first one, we applied a ligand exchange of oleic acid against a water-soluble copolymer obtained by coupling poly(ethylene glycol) to a small branched poly(ethylene imine), PEG−PEI, which has already been employed for CdSe/CdS nanocrystals[13] and will be referred to as "exchange" here. This copolymer ligand consists of a branched PEI moiety with a molecular weight of 400 g/mol and two PEG chains attached to it with molecular weight of 5000 g/mol. We used three different sizes (3, 9, and 18 nm) of nanoparticles in order to investigate size-dependent effects on contrast enhancement. In another approach, the above-mentioned hydrophobic manganese-doped iron oxide nanoparticles were encapsulated within an amphiphilic polymer shell according to Pellegrino et al.,[14] which consists of poly(maleic anhydride-*alt*-1-tetradecene) and is crosslinked by bis(6-aminohexyl)amine. For simplification, we will call it "encapsulation". Finally, we employed an embedding of the nanoparticles into lipid micelles without a ligand exchange. Several block copolymer micelles loaded with iron oxide nanoparticles have recently been demonstrated to act as excellent negative contrast enhancers.[6,15] The different processes are pictured in Scheme 1. The PEG−PEI block copolymer employed for the ligand exchange possesses multiple amino groups that can bind to the particle surface.

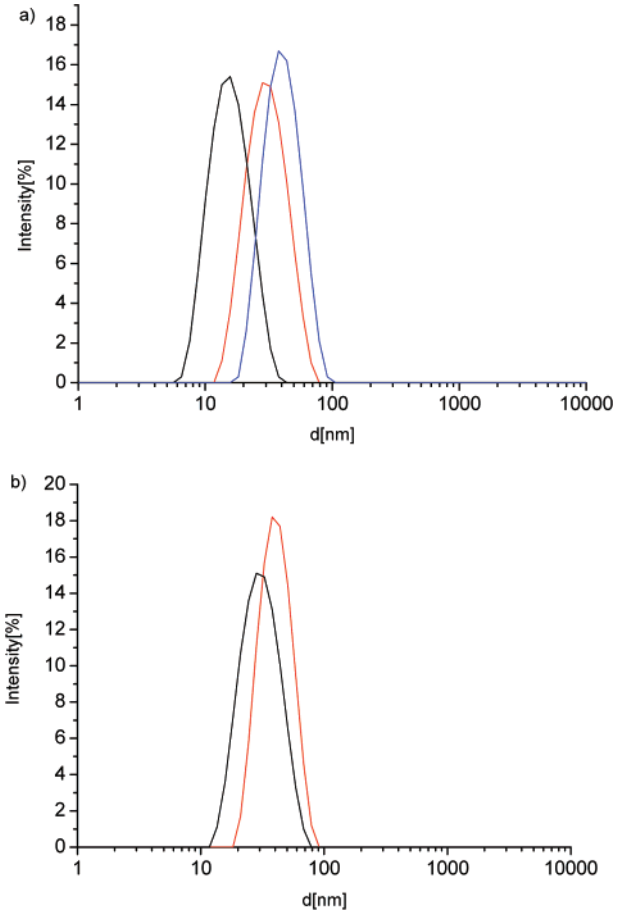

Figure 2. (a) Hydrodynamic diameter of the 9 nm nanoparticles (core size) before (black curve) ligand exchange in chloroform and after ligand exchange with PEG-PEI copolymer in water (red curve) and chloroform (blue curve). (b) Hydrodynamic diameter of PEG-PEI coated particles with 9 nm (black curve) and 18 nm (red curve) core size in water.

To compare the results of ligand exchange to the other approaches, it is essential to know whether the particles are individually dispersed or whether they tend to aggregate. Therefore, we performed dynamic light scattering experiments, the results of which are depicted in Figure 2.

First, it can be noticed from Figure 2a that the hydrodynamic diameter increases after ligand exchange from 15 to 30 nm and 40 nm in water and chloroform, respectively, due to the larger polymer shell. It is further observable that the size distribution of nanoparticles that are covered with PEG−PEI copolymer is not significantly broadened after ligand exchange, indicating that the particles do not tend to form larger agglomerates but exist as individually dispersed particles with a narrow size distribution in both water and chloroform. In addition, Figure 2b shows that the difference in hydrodynamic diameter between nanoparticles with core size of 9 and 18 nm is about 10 nm, demonstrating approximately the same thickness of the polymer shell for particles with different core sizes. Individually dispersed particles were also present after encapsulating the hydrophobic particles in an amphiphilic copolymer shell. This was confirmed by gel electrophoresis and size exclusion chromatography. A TEM image of the as prepared nanoparticles

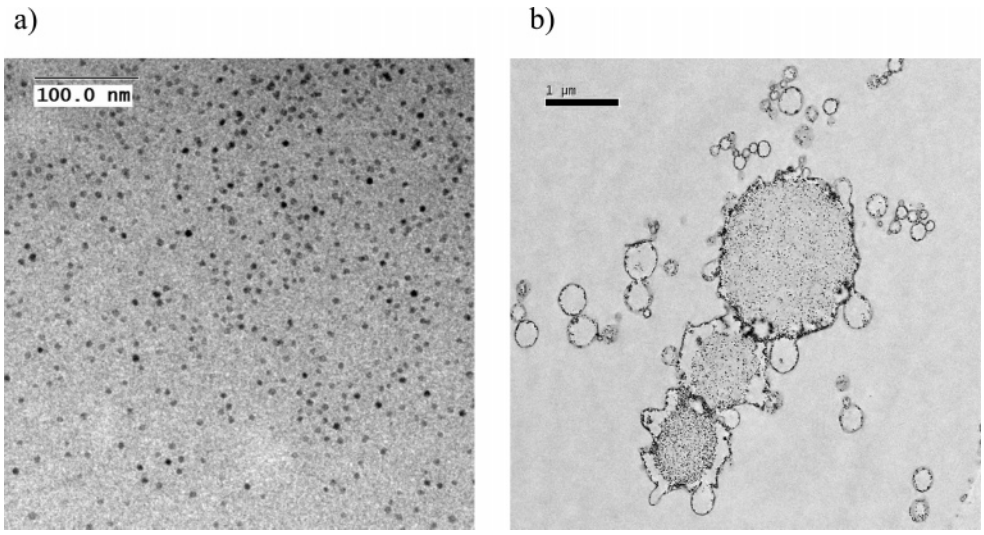

Figure 3. TEM images of manganese-doped iron oxide nanoparticles coated with amphiphilic polymer shell confirming that particles are still well separated after phase transfer (a) and lipid micelles loaded with nanoparticles showing a random distribution within lipid phase and that the particles do not agglomerate within the micelles (b).

is shown in Figure 3a. It is observable that the particles are still well separated after the phase transfer.

The third approach of embedding the particles into lipid micelles differs substantially from the other processes because the particles are concentrated to the small volume in the micellar core. TEM images (Figure 3b) demonstrated the nanoparticles to be randomly distributed inside the micelles. Dynamic light scattering measurements indicated that the micelles are about 250 nm in diameter with a broad size distribution.

To check whether the different postpreparative treatments have a significant influence on the magnetization behavior of the nanocrystals, we measured the magnetic mass susceptibility of 9 nm $MnFe_2O_4$ particles before and after ligand exchange as well as after embedding them into lipid micelles. We found values of 1.5×10^{-4} m^3/kg Fe for both as prepared and after ligand exchange and 1.0×10^{-4} m^3/kg for the micelle sample, respectively. The deviation is rather small and probably within the experimental error of the magnetic measurements and iron analytics.

MRI measurements were carried out on a clinical 3 T magnetic resonance scanner at room temperature, using three different sizes of $MnFe_2O_4$ nanoparticles (3, 9, and 18 nm) with a shell of PEG−PEI copolymer. Furthermore, MRI measurements were accomplished on the 4.5, 6.0, and 7.5 nm manganese-doped iron oxide particles that were transferred into water using Pellegrino's approach, thus forming a comparable system as the particles are individually dispersed in both cases. In contrast, several sizes of $MnFe_2O_4$ and manganese-doped iron oxide nanoparticles were embedded into lipid micelles. As a reference, we measured Resovist (Schering), a commercially used contrast agent, consisting of iron oxide. For further discussion, we will focus on transverse relaxation process. For a T_2* map, reconstructed from T_2*-weighted data from a multiecho gradient echo sequence showing a concentration series of $MnFe_2O_4$ nanoparticles beside a concentration series of Resovist, see Supporting Information Figure S2.

From the experimental values, r_2 and r_2* were determined as exemplarily shown in Figure 4a. Here the reciprocal relaxation times, $1/T_2^* = R_2^*$, defined as the relaxation rates, are plotted versus the concentration of paramagnetic ions. The slopes of these curves yield the concentration independent relaxivities, r_2 and r_2*, respectively, which will be used in the further discussion. These values are plotted in Figure 4b as a function of particle size. All results are also summarized in Table S1 (Supporting Information).

First, it can be noticed from Figure 4b that, in the case of polymer-coated samples, the transverse relaxivities (r_2 and r_2*) increase with increasing particle size for the polymer exchanged and encapsulated particle systems. Figure 4a demonstrates this fact, as the slope of the straight line is higher for larger particles. Furthermore, we observed only small differenes between r_2 and r_2*. In the case of encapsulated particles, one has to take into account that the ratio of iron and manganese increased with increasing particle size for the manganese-doped iron oxides. An effect of changing composition is thus superimposing the size dependence for these particles.

On the other hand, r_2 and r_2* of the particle-loaded micelles were higher than those of the corresponding polymer-coated samples. We also observed significant differences between r_2 and r_2* up to 1 order of magnitude (Figure 4b). The strong decrease in r_2* with increasing particle size is in contrast to the expected behavior. A possible explanation could involve different degrees of particle loading within the micelles. In a control experiment, we investigated different loadings with pure Fe_3O_4 of 6 nm size in order to eliminate size and composition effects. As can be seen from Figure 4c, r_2 and r_2* differ significantly if the loading ratio is changed from 0.025 to 0.05 mg Fe_3O_4 per 1 mg lipid. Thus, the very high r_2* relaxivities for the micelles are probably due to the relatively high particle density within the micelles, which may cause an increased interparticle interaction inside the hydrophobic cores. Such strong particle interactions might be induced by the static

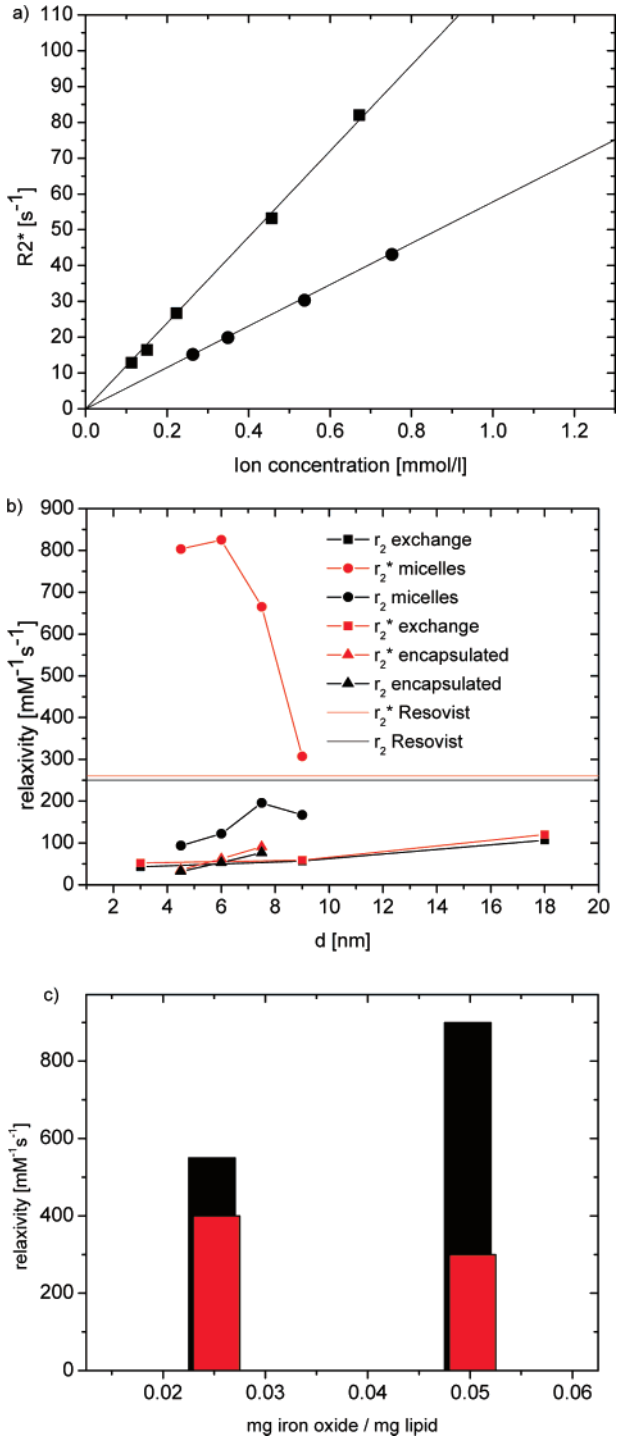

Figure 4. Relaxation rates R_2* for 9 nm (circles) and 18 nm (squares) $MnFe_2O_4$ nanocrystals with respect to a concentration series (a). r_2 (red spots) and r_2* (black spots) for PEG-PEI coated particles (squares), encapsulated particles (triangles) and nanoparticle loaded micelles (circles) (b). Whereas r_2 and r_2* are almost equal in case of homogeneously dispersed particles, r_2* is greatly higher than r_2 for the micelles. r_2 (red bar) and r_2* (black bar) for micelles loaded with different amounts of iron oxide nanoparticles (6 nm) indicating that r_2* increases with increasing loading whereas r_2 slightly decreases (c).

magnetic field of the tomograph. Indeed, we found that even small permanent magnets induce an aggregation of particles in solution. Thus, compartmentalization of nanoparticles in the lipid core of the micelles strongly favors a spacially confined aggregation and thereby produces strong field gradients in the environment.

For the contrast enhancement of magnetic spheres, different regimes are predicted.[16,17] The first one, which is called "motional averaging regime" (MAR) or "motional narrowing regime" describes the transverse relaxation for relatively small particles that are homogeneously dispersed in solution. This theory implies that water diffusion between particles occurs on a much faster time scale than the resonance frequency shift and predicts identical values for R_2 and R_2*. In this regime, the transverse relaxivity increases with increasing particle size. For larger particles, this theory breaks down. In this case, the relaxation rates are given by the "static dephasing regime" (SDR) theory. The SDR, first introduced by Yablonskiy and Haacke,[18] implies that a large magnetic perturber produces strong dipolar fields in its surroundings, the result of which is the fact that, in contrast to the MAR, diffusion has a minimal influence on nuclear magnetic resonance signal decay. The SDR places an absolute limit in the transverse relaxation rate: increasing the perturber size will not result in higher relaxation rates. Thus, a plateau is reached. However, R_2 is always lower than R_2*, reflecting the fact that the use of refocusing pulses in spin−echo sequences leads to a decrease in signal decay ("echo-limiting"), particularly for large magnetic spheres and short echo times. Recently, these regimes have been experimentally demonstrated to exist for an induced clustering process in solution[19] as well as for cells loaded with iron oxides.[20]

The transverse relaxivity for the polymer-coated particles increases with increasing size, thus showing typical behavior of particles in the MAR. r_2 and r_2* should be equal, a condition that is basically fulfilled because the phase loss is mainly caused by diffusion effects in this regime and is thus irreversible with respect to a refocusing pulse. Similar results were obtained for the encapsulated manganese-doped iron oxide nanoparticles. On the other hand, the transverse relaxivities of the micelles are likely to be describable by the "echo-limiting" due to the big differences between r_2 and r_2*. Thus, the ceiling for r_2* given by the SDR should be achieved for the considered systems. For micelles loaded with a higher amount of magnetic nanoparticles, larger r_2* values are observed. This effect is also predicted by SDR theory, as the value of R_2* is proportional to the magnetization of the sphere, i.e., R_2* increases with increasing local magnetic dose (LMD)[18] and thus by particle aggregation. In addition, r_2* is remarkably high, indicating that these micelles could act as powerful negative contrast agents. In this size range, refocusing pulses could be effective and, as a result, r_2 is significantly lower than r_2*. On the other hand, for a further increase in size of the superparamagnetic core of polymer-coated particles, the increase in r_2 and r_2* should be violated at some point due to the decreasing influence of diffusion and thus reaching the SDR condition. Furthermore, the dephasing proton spins of the lipid molecules contribute also to the signal reduction due to the high viscosity of these molecules. This effect has been demonstrated in an experi-

ment where the iron oxide nanoparticles were dispersed in pure olive oil. Large relaxivities were observed in this case. Therefore, the SDR condition is expected to be reached at even smaller perturber sizes within the micelles due to the lower diffusion velocities. Future work will deal with a comprehensive investigation of these effects.

In conclusion, we comparatively investigated the capability of highly crystalline and monodisperse $MnFe_2O_4$ nanoparticles to enhance negative contrast in MRI with respect to appropriate matrices. For these purposes, we applied a ligand exchange with poly(ethylene glycol)-*b*-poly(ethylene imine) copolymer, a coating of hydrophobic nanoparticles with amphiphilic polymer as well as an embedding of nanoparticles into large lipid micelles. We found that, individually, homogeneously dispersed nanoparticles satisfy MAR theory because transverse relaxivities, r_2 and r_2*, increase with increasing core size. On the other hand, if these particles are embedded into lipid micelles, they greatly enhance contrast in T_2*-weighted images, which is in agreement with the static dephasing regime theory. Reasonable explanations for this behavior are the controlled particle aggregation as well as a very low influence of diffusion effects of lipid molecules inside the micelles and water molecules in their surroundings. Further investigations in terms of bioapplicability are currently underway.

Acknowledgment. We thank The Free and Hanseatic City of Hamburg for funding the Molecular Imaging North (MOIN) project. We furthermore thank Rosemarie Kongi, Barbara Holstermann, and Sylvia Bartholdi-Nawrath for excellent technical assistance. Oliver Bruns is supported by a fellowship from the Studienstiftung des Deutschen Volkes.

Supporting Information Available: Detailed experimental procedures and additional data on magnetic and structural characterization. This material is available free of charge via the Internet at http://pubs.acs.org.

References

(1) Bomati-Miguel, O.; Morales, M. P.; Tartaj, P.; Ruiz-Cabello, J.; Bonville, P.; Santos, M.; Zhao, X.; Veintemillas-Veredagner, S. *Biomaterials* **2005**, *26*, 5695.
(2) Huber, D. L. *Small* **2005**, *1*, 482−501.
(3) Jordan, A.; Scholz, R.; Wust, P.; Fahling, H.; Felix, R. *J. Magn. Magn. Mater.* **1999**, *201*, 413−419.
(4) Gonzales, M.; Krishnan, K. M. *J. Magn. Magn. Mater.* **2005**, *293*, 265−270.
(5) Jun, Y. W.; Huh, Y. M.; Choi, J. S.; Lee, H. J.; Song, H. T.; Kim, S.; Yoon, S.; Kim, K. S.; Shin, J. S.; Suh, J. S.; Cheon, J. *J. Am. Chem. Soc.* **2005**, *127*, 5732−5733.
(6) Nasongkla, N.; Bey, E.; Ren. J.; Ai, H.; Khemtong, C.; Guthi, J. S.; Chin, S.-F.; Sherry, A. D.; Boothman, D. A.; Gao, J. *Nano Lett.* **2006**, *6*, 2427−2430.
(7) Huh, Y.-M.; Jun, Y.-W.; Song, H.-T.; Kim, S.; Choi, J.-S.; Lee, J.-H.; Yoon, S.; Kim, K.-S.; Shin, J.-S.; Suh, J.-S.; Cheon, J. *J. Am. Chem. Soc.* **2005**, *127*, 12387.
(8) Taupitz, M.; Schmitz, S.; Hamm, B. *RoeFo, Fortschr. Geb. Roentgenstr. Nuklearmed.* **2003**, *175*, 752.
(9) Perez, J. M.; Josephson, L.; O'Loghlin, T.; Högemann, D.; Weissleder, R. *Nat. Biotechnol.* **2002**, *20*, 816−820.
(10) Berret, J. F.; Schonbeck, N.; Gazeau, F.; El Kharrat, D.; Sandre, O.; Vacher, A.; Airiau, M. *J. Am. Chem. Soc.* **2006**, *128*, 1755.
(11) Lee, J.-H.; Huh, Y.-M.; Jun, Y.-w.; Seo, J.-w.; Jang, J.-t.; Song, H.-T.; Kim, S.; Cho, E.-J.; Yoon, H.-G.; Suh, J.-S.; Cheon, J. *Nat. Med.* **2007**, *13*, 95−99.
(12) (a) Kang, E.; Park, J.; Hwang, Y.; Kang, M.; Park, J.; Hyeon, T. *J. Phys. Chem. B* **2004**, *108*, 13932−13935. (b) Sun, S.; Zeng, H.; Robinson, D. B.; Raoux, S.; Rice, P. M.; Wang, S. X.; Li, G. *J. Am. Chem. Soc.* **2004**, *126*, 273−279.
(13) Nikolic, M. S.; Krack, M.; Aleksandrovic, V.; Kornowski, A.; Förster, S.; Weller, H. *Angew. Chem., Int. Ed.* **2006**, *45*, 6577−6580.
(14) Pellegrino, T.; Manna, L.; Kudera, S.; Liedl, T.; Koktysh, D.; Rogach, A. L.; Keller, S.; Rädler, J.; Natile, G.; Parak, W. J. *Nano Lett.* **2004**, *4*, 703−707.
(15) Ai, H.; Flask, C.; Weinberg, B.; Xintao, S.; Pagel, M. D.; Farrell, D.; Duerk, J.; Gao, J. *Adv. Mater.* **2005**, *17*, 1949−1952.
(16) Gillis, P.; Moiny, F.; Brooks, R. A. *Magn. Reson. Med.* **2002**, *47*, 257−263.
(17) Brooks, R. A.; Moiny, F.; Gillis, P. *Magn. Reson. Med.* **2001**, *45*, 1014−1020.
(18) Yablonskiy, D. A.; Haacke, E. M. *Magn. Reson. Med.* **1994**, *32*, 749−763.
(19) Roch, A.; Gossuin, Y.; Muller, R. N.; Gillis, P. *J. Magn. Magn. Mater.* **2005**, *293*, 532.
(20) Bowen, C. V.; Zhang, X.; Saab, G.; Gareau, P. J.; Rutt, B. K. *Magn. Reson. Med.* **2002**, *48*, 52−61.

NL071099B